Structural and biochemical characterization of two binding sites for nucleation-promoting factor WASp-VCA on Arp2/3 complex

Shih-Chieh Ti[1], Christopher T. Jurgenson[1], Bradley J. Nolen[2], and Thomas D. Pollard[3]

Departments of Molecular, Cellular, and Developmental Biology, Cell Biology, and Molecular Biophysics and Biochemistry, Yale University, New Haven, CT 06520-8103

Edited* by Ronald D. Vale, University of California, San Francisco, CA, and approved May 17, 2011 (received for review January 11, 2011)

Actin-related protein (Arp) 2/3 complex mediates the formation of actin filament branches during endocytosis and at the leading edge of motile cells. The pathway of branch formation is ambiguous owing to uncertainty regarding the stoichiometry and location of VCA binding sites on Arp2/3 complex. Isothermal titration calorimetry showed that the CA motif from the C terminus of fission yeast WASP (Wsp1p) bound to fission yeast and bovine Arp2/3 complex with a stoichiometry of 2 to 1 and very different affinities for the two sites (K_ds of 0.13 and 1.6 μM for fission yeast Arp2/3 complex). Equilibrium binding, kinetic, and cross-linking experiments showed that (*i*) CA at high-affinity site 1 inhibited Arp2/3 complex binding to actin filaments, (*ii*) low-affinity site 2 had a higher affinity for CA when Arp2/3 complex was bound to actin filaments, and (*iii*) Arp2/3 complex had a much higher affinity for free CA than VCA cross-linked to an actin monomer. Crystal structures showed the C terminus of CA bound to the low-affinity site 2 on Arp3 of bovine Arp2/3 complex. The C helix is likely to bind to the barbed end groove of Arp3 in a position for VCA to deliver the first actin subunit to the daughter filament.

crystallography | polymerization | thermodynamics

Members of the Wiskott–Aldrich syndrome protein (WASp) family connect extracellular signals to the assembly of branched actin filaments during cellular motility and endocytosis (1–3). Actin-related protein (Arp) 2/3 complex interacts with the C-terminal VCA domain of a WASp family protein, an actin monomer and an actin filament during the formation of a growing actin filament branch (4, 5).

VCA domains are largely unstructured in solution, but each of their three sequence motifs has different activities. The N-terminal verprolin homology motif (V, a motif also known as WASp homology 2, WH2) forms an α-helix that binds an actin monomer (6). The central motif (C) forms amphipathic helix, which associates mutually exclusively with an actin monomer or Arp2/3 complex (7, 8). The C-terminal acidic motif (A) binds Arp2/3 complex (1). We refer to these motifs as V, C, and A throughout. WASp and N-WASP are auto-inhibited by interactions of VCA with an N-terminal guanosine triphosphatase (GTPase) binding domain (GBD). Association of a Rho-family GTPase with the GBD releases the proteins from autoinhibition (3, 9–11).

The original assumption was that CA binds to a single site on Arp2/3 complex, but several lines of evidence suggest more than one binding site. (*i*) Fusions of WASp-VCA to dimeric glutathione *S*-transferase (GST) (2) and multirepeat VCA regions (12, 13) activate Arp2/3 complex much more strongly than monomeric VCA. (*ii*) Dimers of GST-VCA bind Arp2/3 complex with a stoichiometry of two VCAs to one Arp2/3 complex (13), so Padrick et al. proposed two distinct A binding sites on Arp2/3 complex. (*iii*) Direct or indirect VCA clustering on a membrane can activate Arp2/3 complex even in the absence of a Rho-family GTPase (14–17). (*iv*) A is required for cross-linking VCA to Arp3 (18) and Arp2/3 complex component 1 (ARPC1) (19), but more than 3 nm separate these subunits in crystal structures. (*v*) The N-terminal acidic (NTA) domain of cortactin and VCA bind Arp2/3 complex simultaneously; NTA competes VCA from the cross-linking site on Arp3 but not the cross-linking site on Arp2/ARPC1 (18). (*vi*) Small-angle X-ray solution scattering provided data for a model of Arp2/3 complex with an actin monomer attached to the barbed end of Arp2, V bound to barbed end groove of actin, C bound to the barbed end groove and front of Arp2, and the C-terminal tryptophan of A in a pocket between Arp3 and ARPC3 (20). This orientation of VCA could deliver the second actin subunit of the branch but not the first actin subunit of the daughter filament to the barbed end of Arp3.

Here we address some of the central questions remaining about the pathway of branch formation. Isothermal titration calorimetry (ITC) confirmed that Arp2/3 complex binds two monomeric CAs. Crystal structures of bovine Arp2/3 complex with N-WASp CA show the C-terminal tryptophan binds to subdomain 3 of Arp3. Mutations confirmed that this site is essential for biological function. Formation of an actin filament branch involves more than a dozen different reactions of the VCA domain of WASp with actin monomers and two sites on Arp2/3 complex and between Arp2/3 complex and actin filaments. The only way to map such a complicated pathway is to make quantitative kinetic and thermodynamic measurements of the individual reactions. Using this approach, we found both positive and negative cooperativity among the reactants. Unexpectedly CA bound to high-affinity site 1 inhibits Arp2/3 complex binding to actin filaments, whereas CA binds the second site with much higher affinity when Arp2/3 complex is bound to an actin filament. These observations show that the pathway of actin filament branch formation involves CA binding to two different sites on Arp2/3 complex with opposite effects on actin filament binding.

Results

Evidence for Two Independent CA Binding Sites on Arp2/3 Complex. We used isothermal titration calorimetry to characterize the stoichiometry and thermodynamics of CA binding to Arp2/3 complex. Titration of fission yeast WASp (Wsp1p)-CA into fission yeast or bovine Arp2/3 complex released heat until saturation with more than one CA per Arp2/3 complex (Fig. 1 *A* and *B*). We compared methods to analyze the data. If we floated both

Author contributions: S.-C.T., C.T.J., B.J.N., and T.D.P. designed research; S.-C.T., C.T.J., and B.J.N. performed research; S.-C.T., C.T.J., B.J.N., and T.D.P. analyzed data; and S.-C.T., C.T.J., B.J.N., and T.D.P. wrote the paper.

The authors declare no conflict of interest.

*This Direct Submission article had a prearranged editor.

Data deposition: The atomic coordinates and structure factors have been deposited in the Protein Data Bank, www.pdb.org (PDB ID code 3RSE).

[1]S.-C.T. and C.T.J. contributed equally to this work.

[2]Present address: Department of Chemistry and the Institute of Molecular Biology, University of Oregon, Eugene, OR 97403.

[3]To whom correspondence should be addressed. E-mail: thomas.pollard@yale.edu.

See Author Summary on page 13365.

This article contains supporting information online at www.pnas.org/lookup/suppl/doi:10.1073/pnas.1100125108/-/DCSupplemental.

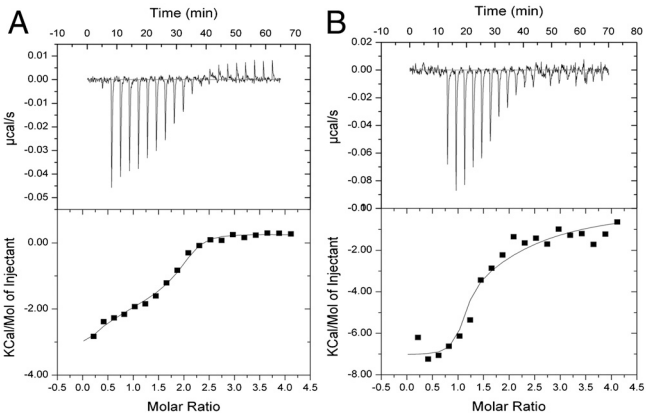

Fig. 1. Measurement of fission yeast Wsp1p-CA binding to Arp2/3 complex by ITC at 25 °C. A 200-µL sample of 8 µM Arp2/3 complex in KMEI buffer [50 mM KCl, 1 mM $MgCl_2$, 1 mM EGTA, 10 mM imidazole (pH 7.0), 1 mM DTT, 0.1 mM ATP] was titrated with 2-µL injections of 160 µM Wsp1p-CA in KMEI at 180-s intervals. Curves are best fits to the data to acquire the stoichiometry and thermodynamic parameters. (*A*) Fission yeast Arp2/3 complex plus fission yeast Wsp1p-CA. (*B*) Bovine Arp2/3 complex plus fission yeast Wsp1p-CA.

the stoichiometry and affinities, the best fits gave stoichiometries of >1.6 with K_ds for the two sites that differed among experiments. A better approach was to fix the stoichiometry at two, which gave more reproducible affinities (Table 1). Fission yeast CA binding to both sites on Arp2/3 complex was exothermic with large positive entropy changes (Fig. 1 and Table 1). Titration of either bovine or fission yeast Arp2/3 complex with bovine CA generated smaller heats than titration with fission yeast CA, but the signal was strong enough to measure the stoichiometry (*SI Text*).

Crystal Structures of CA Bound to Arp2/3 Complex. We used X-ray crystallography to determine high-resolution structures of a small, but informative, part of CA bound to Arp2/3 complex. Key to our success was replacing potassium thiocyanate, previously used in the crystallization buffer, with KCl. Electron density maps of crystals of bovine Arp2/3 complex soaked with >1 mM bovine N-WASP-CA showed three residues (N-WASP-502-EWE-504) from the C terminus of CA bound to Arp3 (Fig. 2*A*). The tryptophan indole ring is sandwiched between Pro236 and the guanidinium moiety of Arg333 (Fig. 2*A*), which are Pro249 and Arg345 in fission yeast. A salt bridge between N-WASP-Glu504 and Arp3-Arg341 is part of an arginine triad with a network of π-stacking interactions with Arg334 and Arg337. Maps of crystals with fission yeast Wsp1-CA had clear density for the C-terminal tryptophan side chain and a single flanking residue. These maps had no density for a second bound CA tryptophan, so the second site identified by ITC may be blocked by crystal contacts.

To test the biological relevance of VCA binding to this site on Arp3, we mutated Pro249 or Arg345 of fission yeast Arp3 (Table 2 and *SI Text*). Deletion of Arp3 is not only lethal but also interferes with sporulation, so that germination of *arp3* :: *ura4*$^+$/*arp3* diploid cells sometimes yields only a single viable spore. Haploid cells depending on Arp3 with mutations P249M, P249A, R345A were not viable, but the Arp3 P249Y mutant grew at 32 and 25 °C as well as wild type. Thus the positive charge of Arg345 and the hydrophobic nature of Pro249 are essential for the biological function of Arp2/3 complex, likely to bind CA, although these residues may also contribute to the structural stability of Arp2/3 complex.

We were surprised to observe two turns of α-helix at the barbed end of Arp3 in $2F_o - F_c$ and $F_o - F_c$ maps of bovine Arp2/3 complex at 2.7-Å resolution both in the presence and absence of CA (Fig. 2*B*), because this helical density was not present in 13 structures of bovine Arp2/3 complex at this resolution (21, 22). This helical density was observed in the original 2.0-Å structure of Arp2/3 complex and interpreted as a helix consisting of ARPC1 residues Ala297 to Ala309 from an adjacent complex in the crystal (23). In our crystals grown in KCl without CA, this density was discontinuous but consistent with the structure of the ARPC1 insert helix. Maps calculated from crystals of bovine Arp2/3 complex with N-WASP-CA or fission yeast Wsp1-CA had the same helical density, most likely attributable to the ARPC1 insert helix. In the following discussion, we suggest that this helical density is a good model for the C helix binding Arp3 (Fig. 2*C*).

VCA Cross-Linked to the Back Side of Arp2 Inhibits Actin Polymerization. Chemical cross-linking showed that the N terminus of VCA is located near Arp2 on the back side of Arp2 adjacent to the EWE binding site on Arp3. Under oxidizing conditions (50 µM $CuSO_4$) bovine N-WASP-VCA with an N-terminal cysteine spontaneously formed a disulfide bond with a cysteine substituted for Arg198 on the top of subdomain 4 of Arp2 of budding yeast Arp2/3 complex (equivalent to Leu199 of Arp2 of bovine Arp2/3 complex; Fig. 3 *A*, lane 5 and *C*). *Schizosaccharomyces pombe* Wsp1p-VCA with an N-terminal cysteine also formed a cross-link to R198C of Arp2 in budding yeast Arp2/3 complex. Under the conditions of these reactions, 10 µM N-WASp-cysteine-VCA should occupy both binding sites on 2 µM *Saccharomyces cerevisiae* Arp2/3 complex, assuming that it binds similar to Wsp1p-CA.

Table 1. Kinetic and thermodynamic parameters of VCA-binding sites on Arp2/3 complex

	Sp Arp2/3 complex	Sp Arp2/3 complex	Bovine Arp2/3 complex	Bovine Arp2/3 complex
	Site 1	Site 2	Site 1	Site 2
K_d, µM	0.13 ± 0.22	1.6 ± 1.33	0.1 ± 0.04	10.1 ± 1.1
ΔH, kcal/mol	−3.3 ± 0.6	−2.3 ± 0.6	−6.9 ± 0.2	−7.5 ± 1.1
ΔS, cal/mol · K	22.7 ± 2.8	19.6 ±4 .2	9.1 ± 0.6	−2.4 ± 3.6
Reaction	K_d, µM	k_-, s^{-1}	k_+, M^{-1} s^{-1}	
Sp Arp2/3 complex+ unlabeled CA	0.29 (measured by competition with labeled CA)			
Sp Arp2/3 complex+ labeled CA	0.018 (measured)	28 (measured)	1.5×10^9 (calculated from K_d and k_-)	
Sp Arp2/3 complex-actin filaments + unlabeled CA	0.049 (measured by competition with labeled CA)			
Sp Arp2/3 complex- actin filaments + labeled CA	0.008 (measured)	22 (measured)	2.7×10^9 (calculated from K_d and k_-)	

Equilibrium binding of fission yeast (Sp) Wsp1p-CA to fission yeast (Sp) or bovine Arp2/3 complex measured by five independent isothermal titration calorimetry experiments, assuming two binding sites while fitting the data (Fig. 1). Fluorescence anisotropy measurements of rate and equilibrium constants for fission yeast Wsp1p-CA binding fission yeast Arp2/3 complex in the presence and absence of actin filaments.

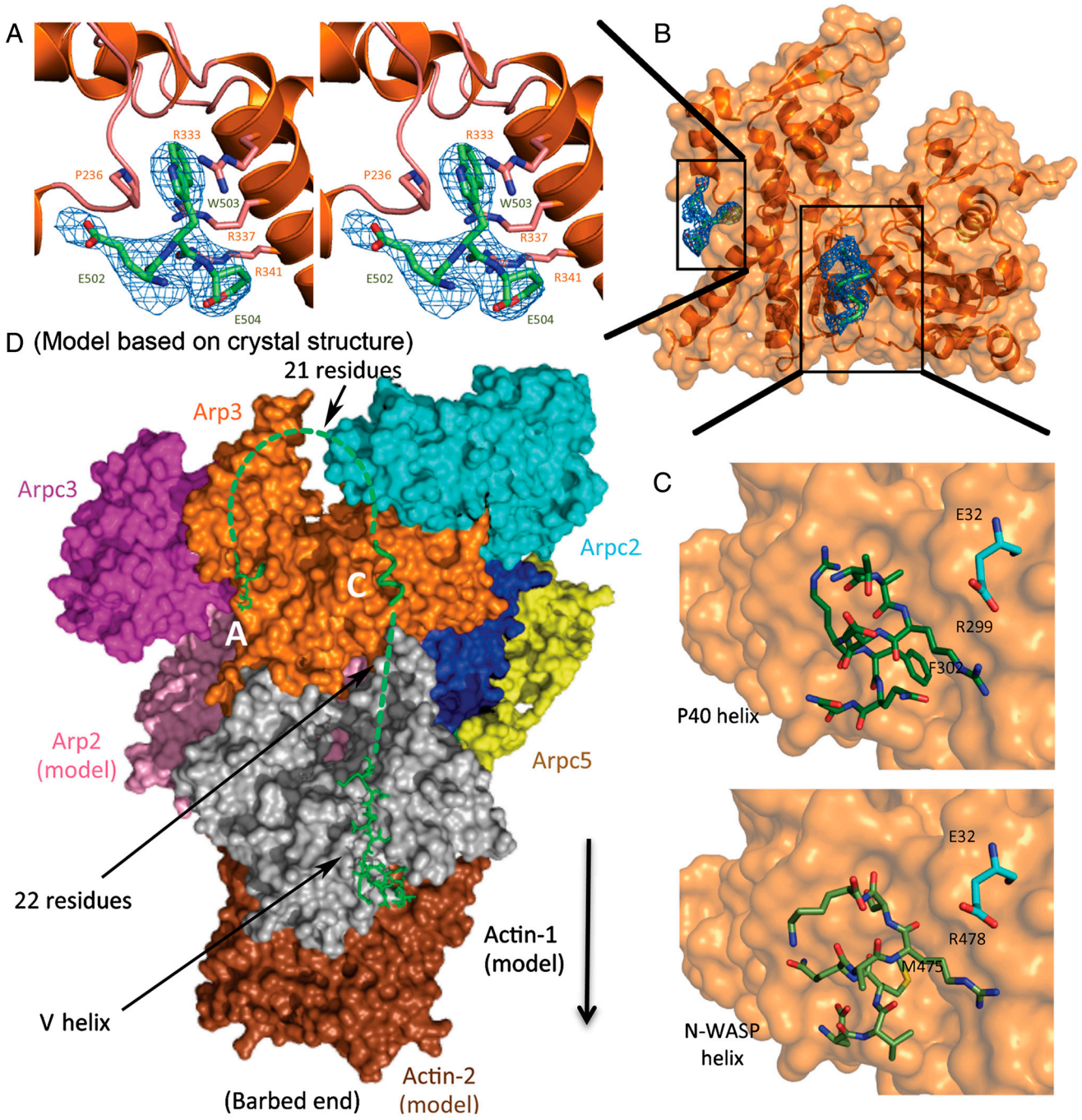

Fig. 2. Crystal structures and models of WASp-CA bound to bovine Arp2/3 complex. (*A*) Stereo diagram of a $2F_o - F_c$ density map (blue) of the C-terminal A-tripeptide (lime-green stick figure) bound to Arp3 (orange ribbon diagram). (*B*) Space-filling model and ribbon diagram of Arp3 (orange) and the density (blue) from a $2F_o - F_c$ map contoured to 1σ of the C-terminal A-tripeptide (lime-green stick figure) and the ARPC1 insert helix (backbone green) at the barbed end of Arp3. (*C*) Space-filling model of Arp3 with stick figures (*Upper*) of the structure of the ARPC1 insert helix (dark green) and (*Lower*) a homology model of the N-WASP C helix (lime green) in the same location. Residue E32 from ARPC2 is cyan. (*D*) Hypothetical model based on crystal structures for VCA associating with Arp2/3 complex at site 2 and the first two subunits of the daughter filament. A Holmes actin filament model was aligned with Arp3 to position Arp2 (pink) and the first (gray) and second (brown) subunits of the daughter filament. The elements of VCA are shown as follows: The backbone (green) of the C-terminal A-tripeptide and the C helix (Fig. 2*C*) are associated with Arp3 and a stick figure of human WASp-V (green) (Protein Data Bank ID code 2A3Z) is bound to the first actin subunit. Dashed green lines represent 21 residues of the A loop and 22 residues in the V-C connector. A black arrow indicates the direction of the growing daughter filament.

Control experiments showed that N-WASP-cysteine-VCA does not form disulfides with the cysteine substitution L155C in Arp3 (equivalent to Leu117 of Arp3 of bovine Arp2/3 complex; Fig. 3*A*, lane 4) or Arp2/3 complex with other cysteine substitutions (Arp2 D271C, Arp3 P342C; or Arp2 A207C, Arp3 D325C). Bovine N-WASP-VCA with a C-terminal cysteine did not form a disulfide bond with either Arp2 or Arp3 carrying these cysteine substitutions.

Purified Arp2/3 complex cross-linked to VCA did not stimulate actin filament nucleation like mixtures of VCA and Arp2/3 complex, unless the disulfide bond was reduced (Fig. 3*B*). The cross-link is likely to preclude the 30-Å movement of Arp2 rela-

Table 2. Spore viability of diploid fission yeast with Arp3 mutations

No. of viable spores per ascus	Δarp3	Arp3 P249A	Arp3 R345A	Arp3 P249M
1	22	2	1	2
2	14	34	35	34
3	0	0	0	0
4	0	0	0	0

For each strain, 36 asci were picked, and the viable spores were counted after incubating on YE5S agar plate at 25 °C for 4 d.

tive to Arp3 during activation of the complex and/or the cross-link may prevent V from delivering the first actin subunit to the daughter filament.

Actin Filaments Increase the Affinity of Arp2/3 Complex for WASp-CA. We used fluorescence anisotropy to measure CA binding to free Arp2/3 complex and Arp2/3 complex bound to the side of a filament. We labeled a cysteine added to the N terminus of CA with maleimide-Alexa-Fluor-546. Alexa-Fluor-546-labeled CA alone has a fluorescence anisotropy of approximately 0.2, and titration of low concentrations (<10 nM) of labeled Wsp1p-CA with Arp2/3 complex increased the fluorescence anisotropy to 0.36. The clean, single-site binding isotherms gave K_ds of Arp2/3 complex and Alexa-Fluor-546-CA of 18.4 nM (average of 11 and 25.8 nM) without actin filaments and 7.9 nM (average of 4 and 11.7 nM) with 5 μM actin filaments (Fig. 4*A* and Table 1).

We competed unlabeled CA with Alexa-Fluor-546-Wsp1p-CA to determine the affinity of the unlabeled Wsp1p-CA for the high-affinity site 1 on Arp2/3 complex. Given the low concentration of Alexa-Fluor-546-CA, we assumed that all the labeled CA was bound to the high-affinity site 1 on Arp2/3 complex and that interactions of Wsp1p-CA with the two binding sites are independent of each other. Fitting the data gave the upper limit K_d of the high-affinity site 1, because a small fraction of the unlabeled Wsp1p-CA may have been bound to the low-affinity site 2 (Fig. 4*B*). Unlabeled CA bound Arp2/3 complex with a K_d of 0.29 μM (average of 0.30 and 0.28 μM), similar to the affinity of unlabeled Wsp1p-CA for site 1 measured by ITC (0.13 μM) and of human WASp-VCA for bovine Arp2/3 complex (24).

The affinity of unlabeled CA for Arp2/3 complex was higher in the presence of actin filaments, with a K_d of 0.05 μM (average of 0.073 and 0.025 μM) (Fig. 4*B* and Table 1). Because filaments block and inhibit CA binding at high-affinity site 1 on Arp2/3 complex (data shown in Fig. 6*A*), we interpret this to mean CA has higher affinity for site 2 when Arp2/3 complex is bound to an actin filament.

We measured the rate of dissociation of Alexa-Fluor-546-labeled CA from Arp2/3 complex after mixing with excess unlabeled CA. The reaction reached equilibrium within 1 s, giving dissociation rate constants of 22 s^{-1} without actin filaments (presumably site 1) and 28 s^{-1} with actin filaments (presumably site 2) (Fig. 4*C* and Table 1). These dissociation rates may have been faster than the reported rate constant of 0.3 s^{-1} for dissociation of rhodamine-WASP-VCA from bovine Arp2/3 complex (24), because the experiments used different species of VCA labeled with different dyes.

Arp2/3 Complex Has a Much Higher Affinity for CA than Actin-VCA. To study how an actin monomer bound to VCA influences its interactions with Arp2/3 complex, we used *N*,*N*′-m-phenylenedimaleimide to cross-link a cysteine on the N terminus of Wsp1p-VCA to Cys374 of actin monomers labeled on lysine with Alexa-Fluor-488 (6, 20) (Fig. 5*A*). This strategy allowed for experiments uncomplicated by dissociation of actin from VCA.

Measurements of fluorescence anisotropy showed that different concentrations of Arp2/3 complex were required to bind CA and actin-VCA and that Arp2/3 complex bound to actin filaments has a higher affinity for actin-VCA than free Arp2/3 complex (Fig. 5*B*). Titration of 20-nM cross-linked Alexa-Fluor-488-actin-VCA with Arp2/3 complex increased the fluorescence anisotropy. Lower concentrations of Arp2/3 complex bound to actin filaments were required to increase the anisotropy and even lower concentrations of free Arp2/3 complex increased the anisotropy of Alexa-Fluor-488-CA.

Saturating the binding sites in the experiments was challenging owing to limited quantities of free Arp2/3 complex and Arp2/3 complex bound to actin filaments. We measured anisotropies up to 0.36 at 13 μM free Arp2/3 complex (see *SI Materials and Methods*), but higher concentrations of Arp2/3 complex were

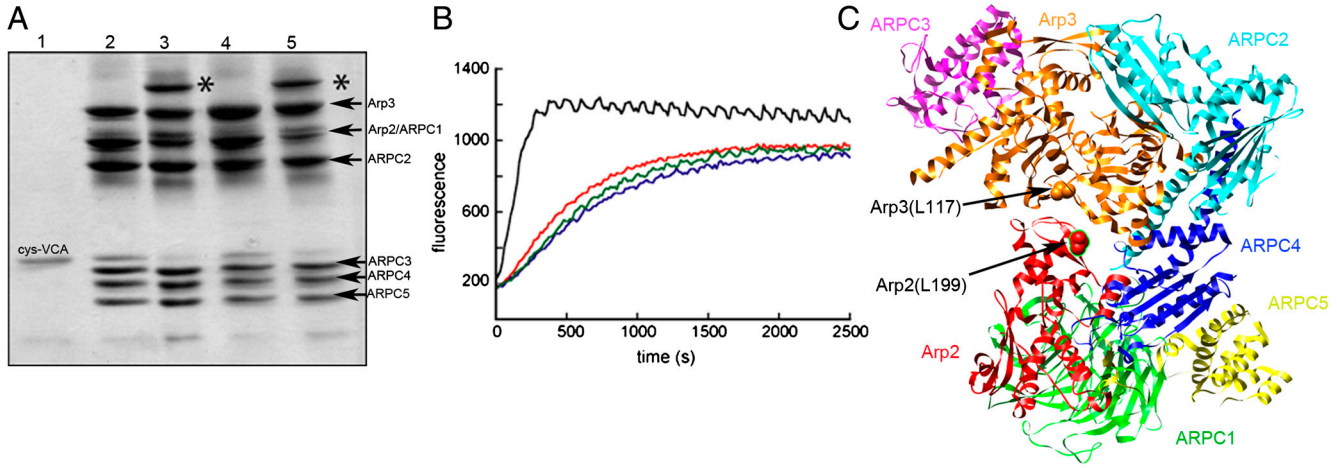

Fig. 3. Cross-linking a cysteine at the N terminus of N-WASp-VCA to R198C in subdomain 4 of Arp2 of budding yeast Arp2/3 complex. (*A*) SDS-PAGE without a reducing agent of cross-linking reaction products. Lanes 1, N-WASp-cysteine-VCA; 2, wild-type Arp2/3 complex plus N-WASp-cysteine-VCA; 3, Arp2/3 complex with mutations Arp3 (L155C) and Arp2 (R198C) plus N-WASp-cysteine-VCA; 4, Arp2/3 complex with Arp3 (L155C) plus N-WASp-cysteine-VCA; 5, Arp2/3 complex with Arp2 (R198C) plus N-WASp-cysteine-VCA. * VCA cross-linked to Arp2. (*B*) *Saccharomyces cerevisiae* (Sc) Arp2/3 complex cross-linked to N-WASp-VCA does not nucleate actin filaments. Time course of actin polymerization monitored by the fluorescence of pyrene-labeled actin. Conditions: 4 μM actin (15% pyrene-labeled), 10 mM imidazole (pH 7.0), 50 mM KCl, 1 mM $MgCl_2$, 1 mM EGTA, 0.2 mM ATP, 0.2 mM $CaCl_2$. Red, actin alone; blue, actin incubated for 5 min with 10 mM DTT; green, 100 nM ScArp2/3 complex Arp3 (L155C)/Arp2 (R198C) cross-linked to N-WASp-cysteine-VCA; black, 100 nM ScArp2/3 complex Arp3 (L155C)/Arp2 (R198C) cross-linked to N-WASp-cysteine-VCA incubated with 10 mM DTT for 5 min. (*C*) Ribbon diagram of bovine Arp2/3 complex (Protein Data Bank ID code 1TYQ) with red spheres showing Arp2 L199 (equivalent to R198 of ScArp2) and orange spheres showing Arp3 L117 (equivalent to L155 of ScArp3). Subdomains 1 and 2 of Arp2 lacked electron density and are not included.

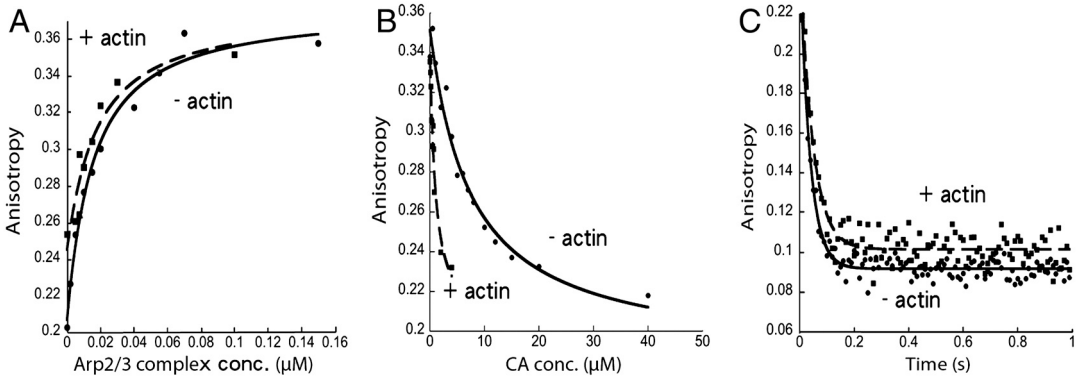

Fig. 4. Actin filaments increase the affinity of fission yeast Arp2/3 complex for Wsp1p-CA. (*A*) Fluorescence anisotropy assays of equilibrium binding of Alexa-Fluor-546 labeled CA to Arp2/3 complex. (●) 2.7 nM Alexa-Fluor-546-Wsp1p-CA titrated with Arp2/3 complex or (■) 10 nM Alexa-Fluor-546-Wsp1p-CA with 5 μM actin filaments titrated with Arp2/3 complex previously equilibrated for 8 h with 5 μM actin filaments. Each data point is an average of four measurements. (*B*) Fluorescence anisotropy assays for equilibrium competition between unlabeled Wsp1p-CA and Alexa-Fluor-546-Wsp1p-CA for binding to Arp2/3 complex. Titration with unlabeled Wsp1p-CA of (●) 2.7 nM Alexa-Fluor-546-Wsp1p-CA and 0.4 μM Arp2/3 complex or (■) 10 nM Alexa-Fluor-546-Wsp1p-CA, 5 μM actin filaments and 0.1 μM Arp2/3 complex. (*C*) Fluorescence anisotropy measurement of the time course of dissociation of Alexa-Fluor-546-Wsp1p-CA from Arp2/3 complex after mixing with an equal volume of unlabeled Wsp1p-CA. (●) Mixing 200 μM unlabeled Wsp1p-CA with 1.5 μM Arp2/3 complex and 1 μM Alexa-Fluor-546-Wsp1p-CA. The average of 14 time courses from two experiments gave $k_{obs} = 27.6\ s^{-1}$. (■) Mixing 80 μM unlabeled CA with 0.5 μM Arp2/3 complex, 0.4 μM Alexa-Fluor-546-Wsp1p-CA, and 13, 22.5, or 25 μM actin filaments. The average of 14 time courses from three experiments with three actin concentrations gave $k_{obs} = 21.8\ s^{-1}$.

not available to reach a plateau. To calculate the fraction of cross-linked Alexa-Fluor-488-actin-VCA bound to each concentration Arp2/3 complex, we assumed that the upper limit of fluorescence anisotropy of randomly oriented molecules in water solution is 0.4, so the highest fluorescence anisotropy in our titration corresponded to about 70% (average of 52% and 88% in two experiments) of actin-VCA bound to Arp2/3 complex. By the same criterion, about 28% (average of 15% and 40%) of actin-VCA bound to 0.1 μM Arp2/3 complex associated with 5 μM actin filaments (Fig. 5*B*), the highest concentration of this material available (see *SI Materials and Methods*). The semilog graph in Fig. 5*B* shows that Arp2/3 complex has a much higher affinity for Alexa-Fluor-546-labeled CA than actin-VCA, and that actin-VCA has a higher affinity for Arp2/3 complex bound to actin filaments (estimated $K_d = 0.1$ μM) than free Arp2/3 complex (estimated $K_d = 10$ μM).

Polymerization assays with pyrene-labeled actin showed that cross-linked actin-VCA was less active than VCA in promoting the nucleation of actin filaments (Fig. 5*C*). A concentration of 500 nM actin-Wsp1p-VCA produced the same rate of polymerization as 50–100 nM monomeric Wsp1p-VCA. When half of the actin monomers were polymerized, 500 nM actin-Wsp1p-VCA produced 0.4-nM ends and 500 nM monomeric Wsp1p-VCA produced 1.7-nM ends from 50 nM Arp2/3 complex.

CA Inhibits Binding of Arp2/3 Complex to the Side of Actin Filaments. We used a fluorescence assay to measure binding of pyrene-labeled Arp2/3 complex to the sides of actin filaments. Addition of actin filaments to fission yeast Arp2/3 complex with a pyrene label on A317C of ARPC2 results in a slow increase in the fluorescence signal (Fig. 6*A*), which is interpreted as Arp2/3 complex binding to the sides of actin filaments (25). Time courses of the fluorescence change following mixing of 0.2 μM pyrene-labeled

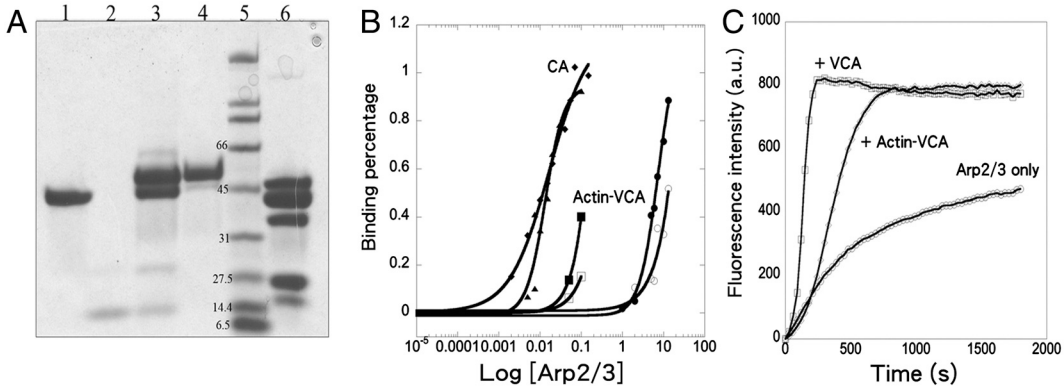

Fig. 5. Interactions of fission yeast Arp2/3 complex with Wsp1p-CA and Wsp1p-VCA cross-linked to actin monomer. (*A*) Purification of fission yeast Wsp1p-VCA cross-linked to Alexa-Fluor-488-actin monomer. SDS-PAGE of samples, Lanes: 1, Alexa-Fluor-488-actin monomer; 2, cys-VCA reacted with PDM; 3, VCA cross-linked to Alexa-Fluor-488-actin monomer before purification; 4, Alexa-Fluor-488-actin-VCA purified from free actin and VCA by gel filtration and Mono Q chromatography; 5, protein standards with molecular weights; 6, fission yeast Arp2/3 complex. (*B*) Fluorescence anisotropy assay of equilibrium binding of fission yeast Wsp1p-CA or Wsp1p-VCA cross-linked to an actin monomer to fission yeast Arp2/3 complex ±5 μM actin filaments. Samples were incubated for 4 min at 25 °C with a range of concentrations of Arp2/3 complex and (◆) 2.7 nM Alexa-Fluor-546-Wsp1p-CA, (▲) 10 nM Alexa-Fluor-546-Wsp1p-CA with 5 μM actin filaments, (●, ○) two independent experiments with 20 nM Alexa-Fluor-488-actin-VCA, or (■, □) two independent experiments with 20 nM Alexa-Fluor-488-Actin-VCA with 5 μM actin filaments. (*C*) Nucleation-promoting activity of VCA and VCA cross-linked to actin monomer assayed by the time course of polymerization of pyrene-labeled actin. Conditions: 2.5 μM 15% pyrene-labeled actin monomers and 50 nM fission yeast Arp2/3 complex in KMEI buffer [50 mM KCl, 1 mM $MgCl_2$, 1 mM EGTA, 10 mM imidazole (pH 7.0), 1 mM DTT, 0.1 mM ATP] with (○) no additions, (□) 500 nM Wsp1p-VCA, or (◇) 500 nM Wsp1p-VCA cross-linked to actin monomer.

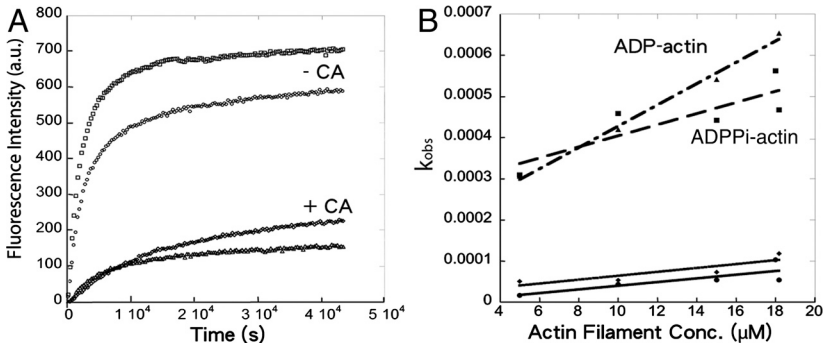

Fig. 6. Wsp1p-CA inhibits binding of fission yeast Arp2/3 complex to the side of actin filaments. (*A*) Time course of pyrene-labeled fission yeast Arp2/3 complex binding to actin filaments measured by fluorescent intensity. Conditions: KMEI buffer [50 mM KCl, 1 mM $MgCl_2$, 1 mM EGTA, 10 mM imidazole (pH 7.0), 1 mM DTT, 0.1 mM ATP] with 16.7 mM K_2SO_4 to form ADP-actin filaments or 16.7 mM potassium phosphate to form ADP · P_i-actin filaments. Reactions of 0.2 μM pyrene-labeled Arp2/3 complex with (○) 15 μM ADP-actin filaments or (□) 15 μM ADP · P_i-actin filaments. Reactions of 0.2 μM pyrene-labeled Arp2/3 complex and 1 μM Wsp1p-CA with (◇) 15 μM ADP-actin filaments or (△) 15 μM ADP · P_i-actin filaments. (*B*) Actin filament concentration dependence of k_{obs} from pyrene-labeled Arp2/3 complex binding ADP- and ADP · P_i-actin filaments. Data from *A* were fit to two exponentials, a large amplitude fast reaction and a small amplitude slow reaction. Slopes of these plots give k_+ and the *y* intercepts give k_-. Fast components: (▲) ADP-actin filaments, and (■) ADP · P_i-actin filaments. Slow components: (◆) ADP-actin filaments, and (●) ADP · P_i-actin filaments.

Arp2/3 complex with a range of actin filament concentrations could be fit with double exponential equations. With ADP-actin filaments, k_{obs} for the faster, large-amplitude component was proportional to actin filament concentration (Fig. 6*B*), giving $k_+ = 3 \times 10^{-5}$ μM^{-1} s^{-1}, $k_- = 2 \times 10^{-4}$ s^{-1}, and $K_d = 6.7$ μM. For ADP · P_i-actin filaments, the parameters were $k_+ = 1 \times 10^{-5}$ μM^{-1} s^{-1}, $k_- = 3 \times 10^{-4}$ s^{-1}, and $K_d = 30$ μM (Fig. 6*B*). The k_{obs} values for the slower reactions depended weakly on the actin filament concentration (Fig. 6*B*). The source of the signal for the slow reaction is not known.

Two aspects of these results deserve comment. First, both the association and dissociation rate constants were 10-fold smaller in our assays than Beltzner and Pollard (25). We discovered that photobleaching of pyrene in the previous work caused the fluorescence change to plateau prematurely. These truncated time courses gave falsely high values of k_{obs} for the binding reactions. Lower intensity excitation used here reduced photobleaching and allowed us to observe higher amplitudes of fluorescence change over longer time courses with lower k_{obs}.

Second, the higher affinity of Arp2/3 complex for ADP-actin filaments ($K_d = 6.7$ μM) than ADP · P_i-actin filaments ($K_d = 30$ μM) was surprising given that branches appeared to be more stable on ADP · P_i-actin filaments than on ADP-actin filaments (26). A simple hypothesis to explain all of the data is that the presence of a daughter filament influences the affinity of Arp2/3 complex for ADP · P_i- and ADP-actin filaments.

The presence of 1 μM CA dramatically decreased the initial rate for Arp2/3 complex association with 15 μM actin filaments from 0.10 to 0.016 arbitrary units (ADP · P_i-actin filaments) and from 0.14 to 0.013 arbitrary units (ADP-actin filaments) (Fig. 6*A*). Because 1 μM CA saturates the high-affinity site 1 but not all of low-affinity site 2, this result is evidence that CA occupancy of the high-affinity site 1 interferes directly or indirectly with Arp2/3 complex binding to actin filaments. These slow reactions did not reach a plateau in 12 h with either ADP- or ADP · P_i-actin filaments (Fig. 6*A*), so we could not measure equilibrium binding of CA-Arp2/3 complex to actin filaments with this assay.

Discussion

Our ITC measurements confirm the 2:1 stoichiometry of CA binding to Arp2/3 complex (13) and together with our spectroscopic binding assays provide the only evidence that the affinities of CA for the two sites differ more than 10-fold (Table 1). Reactions of Wsp1p-CA with both sites on Arp2/3 complex are exothermic with large positive entropy changes, so both hydrophobic and electrostatic interactions are involved, as expected from the participation of the acidic residues of the A motif and the hydrophobic nature of both the conserved tryptophan residue in A motif and the amphipathic helix formed by the C motif (7, 24). Our crystal structures and cross-linking VCA to Arp2/3 complex show one binding site on the back side of Arp2/3 complex, which is probably low-affinity binding site 2 that delivers the first subunit to the daughter filament as proposed in the model in Fig. 2*D*. Cross-linking CA to Arp2 (8, 18, 27, 28) showed that Arp2 on the front side of Arp2/3 complex participates in the high-affinity site 1. Our kinetic and thermodynamic data show that association of Arp2/3 complex with the side of an actin filament strongly influences CA binding to both sites and that actin monomer bound to V influences the binding of VCA to Arp2/3 complex. We first consider the two binding sites and then the reaction mechanism.

High-Affinity CA Binding Site 1 on Arp2/3 Complex. Multiple independent lines of evidence show that high-affinity site 1 is on the front side of Arp2/3 complex and ARPC1 contributes much of the binding energy. (*i*) A can be cross-linked to ARPC1 (8, 18, 27, 28). (*ii*) GST-VCA has nearly the same affinity for purified ARPC1 and Arp2/3 complex (19). (*iii*) High concentrations of VCA reduced hydrogen/deuterium exchange of two ARPC1 peptides (29). (*iv*) The affinity of VCA for ΔArp2 Arp2/3 complex (lacking Arp2) is similar to that for complete Arp2/3 complex (30).

Multiple studies also agree that CA can be covalently cross-linked to Arp2 by a variety of strategies (8, 18, 27, 28), but locating this site has been problematic. Cross-linking has not identified this binding site and the evidence from other approaches is not yet self-consistent.

The pointed end of Arp2 is one possible binding site given that a high concentration (160 μM) of WASp-VCA also reduced hydrogen/deuterium exchange of peptides that form helices and loops in subdomains 2 and 4 at the pointed end of Arp2 (29). Direct binding was judged to be more likely to cause these changes than movement of Arp2 relative to Arp3. Our crystals soaked in CA had no extra density at the pointed end of Arp2, most likely because crystal contacts blocked this binding site. VCA at this position should interfere directly with Arp2/3 complex binding to the side of an actin filament as observed in our spectroscopic assays.

The barbed end groove is another potential binding site for C on Arp2, as proposed in a model based on small angle X-ray scattering of actin-VCA bound to Arp2/3 complex (20) and supported by the effects of high concentrations of VCA hydrogen/deuterium exchange on residues in this groove of Arp2 (29). On the other hand, no density for C appeared in the barbed end groove of Arp2 in our electron density maps. One possibility is that CA occupies

more than one site on Arp2 at different points in the branching pathway.

Low-Affinity CA Binding Site 2 on Arp2/3 Complex. Our crystal structures are the only high-resolution information about CA binding to Arp2/3 complex. They show why interaction of the conserved tryptophan at the C terminus of A with Arp3 is required for CA binding to Arp2/3 complex (24), cross-linking to Arp3 (18, 19), and viability of fissions yeast (see *SI Text*).

Although the ARPC1 insert helix occupied the hydrophobic groove at the barbed end of Arp3 in our crystals, this is also an attractive site to bind the C helix (7). The ARPC1 insert helix has a hydrophobic residue Phe302 separated by two residues from an arginine, similar to the two most conserved residues in the C motif, a hydrophobic residue (Φ) and an arginine (R) separated by two residues in the consensus sequence ΦXZXΦXZXΦXX RXXΦ (7). Mutation of either of these residues reduces nucleation-promoting activity (7).

When modeled into the ARPC1 helical density with the opposite polarity, N-WASP-C (residues 473-EV**M**QA**R**SK-480) shares three features with the ARPC1 insert helix (Fig. 2*C*). First, the side chains of N-WASP-Met475 and ARPC1-Phe302 make van der Waals interactions with a hydrophobic pocket consisting of Arp3 residues Trp153, Phe379, and Met383. Second, the guanidinium moieties of CA-Arg478 and ARPC1-Arg299 are close to ARPC2-Glu32. Third, like ARPC1-Arg301, residues Glu473 and Gln476 of the C helix may donate hydrogen bonds to the backbone oxygen atoms of Arp3 Ser155 and Val158 in a surface loop (155-SRQVG-159) with density in the 2.0 Å Arp2/3 complex structure (23) but not in other structures of Arp2/3 complex (21, 22). This loop may be an adaptation of Arp3 to bind CA, because it is missing in actin.

In this model (Fig. 2*D*), the three elements of VCA are positioned to deliver the first actin subunit of the daughter filament to the barbed end of Arp3 next to Arp2 (5, 31, 32). The V helix is bound at the barbed end of the first actin subunit (6) and connected to the C helix by 22 residues. Arp2/3 complex on a mother

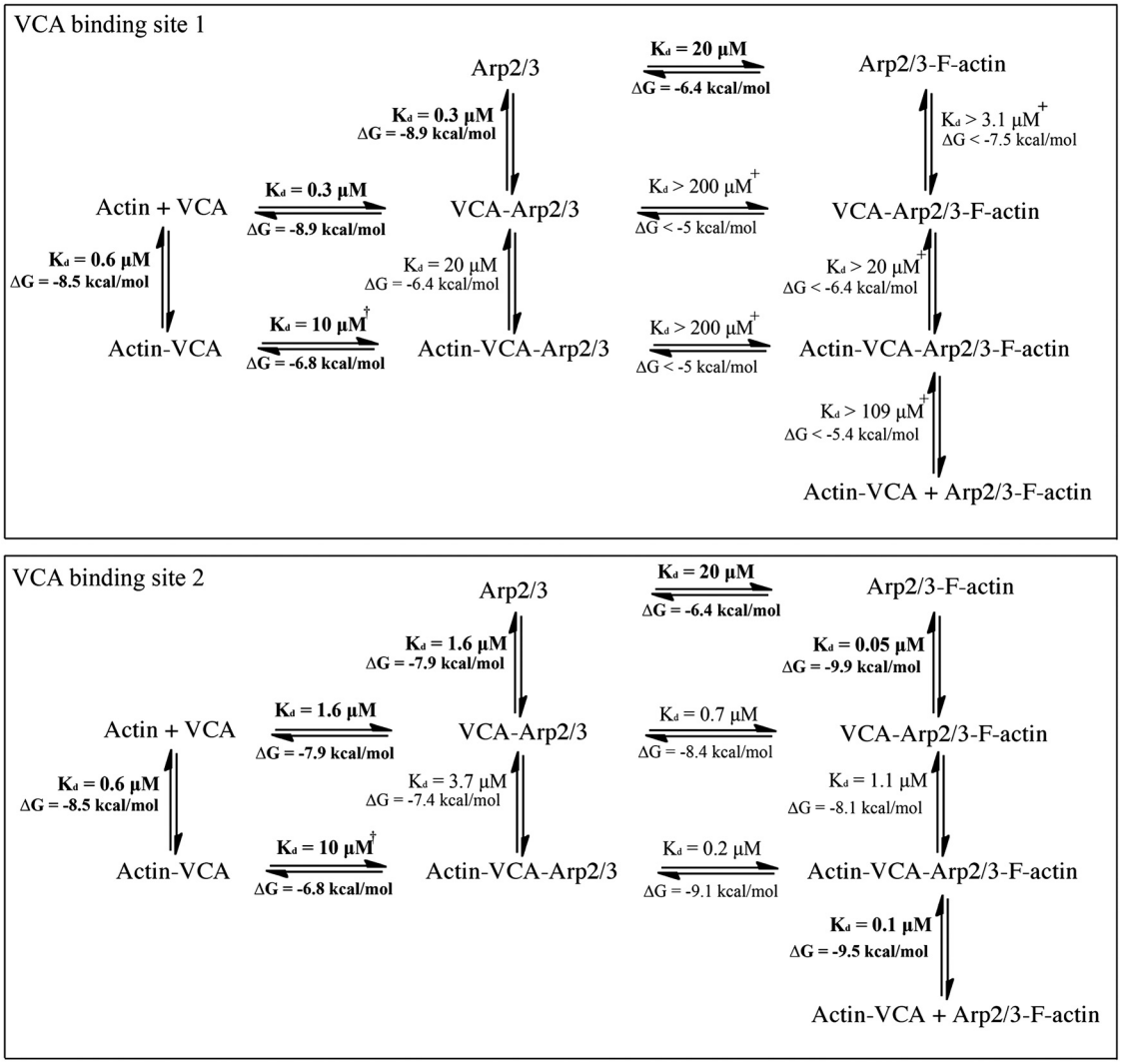

Fig. 7. Thermodynamics of the interactions of VCA, Arp2/3 complex, actin monomer, and mother actin filament. The top rows are Arp2/3 complex alone. The second rows are Arp2/3 complex with VCA. The thirds rows are Arp2/3 complex with actin-VCA. The left columns are without Arp2/3 complex. The middle columns are Arp2/3 complex without actin filaments. The right columns are Arp2/3 complex bound to actin filaments. Scan vertically or horizontally to see the effects of each bound ligand on binding of other ligands. The K_ds are from experimental measurements (this paper; 24; in bold font) or from the detailed balance calculations. The + symbol indicates reactions where limits were estimated and the † symbol indicates uncertainty about whether VCA cross-linked to actin binds site 1 or site 2. Binding of CA to site 1 interferes with Arp2/3 complex binding to the sides of actin filaments. CA binding to site 2 on Arp2/3 complex promotes binding of the complex to the sides of actin filaments. The free energy change ΔG during formation of the actin-VCA-Arp2/3 complex on the side of an actin filament from the four reactants is −24.4 kcal/mol.

filament would have higher affinity for actin-VCA (Fig. 5*B*), because Arp2 would be positioned more favorably for binding the first actin than in free Arp2/3 complex. Exposure of this entire CA binding site in the EM model of the branch junction (5) explains why the mother filament does not compete for binding to site 2. The model explains why VCA can be cross-linked to Arp3 and ARPC3 and less readily to ARPC2 and ARPC5 (8, 18, 27, 28) and how the N terminus of V can be cross-linked to the back side of subdomain 4 of Arp2 (Fig. 3). VCA binding reduces hydrogen/deuterium exchange in two Arp3 peptides in the proposed C helix binding site, but not residues around the A binding site observed in our crystals (29). Our hypothesis is consistent with NMR observations and mutagenesis (7), although it is not known which CA binding site was probed in those experiments.

Positive and Negative Interactions Among the Proteins at Branch Junctions. The components that assemble branches—actin monomers, actin filaments, VCA, and Arp2/3 complex—have both positive and negative influences on the interactions of other components as illustrated by the free energy changes associated with these reactions (Fig. 7). When Arp2/3 complex is bound to a mother filament, site 2 has a 40-fold higher affinity for CA than free Arp2/3 complex. Similarly, Arp2/3 complex on a mother filament binds VCA cross-linked to an actin monomer with much higher affinity (presumably for site 2) than free Arp2/3 complex. Therefore, by detailed balance, CA or actin-VCA binding to site 2 should increase the affinity of Arp2/3 complex for actin filaments 40- to 100-fold. Conformational changes may explain this difference. The barbed end grooves and nucleotide-binding clefts of actin-family proteins open and close in a reciprocal fashion. The nucleotide-binding cleft of Arp3 is open and the groove is closed in inactive Arp2/3 complex. The nucleotide-binding cleft of Arp3 is closed in the model of the branch junction (5), so the Arp3 barbed end groove is expected to be open and may be more favorable for binding the C helix.

Other interactions have negative effects on linked reactions (Fig. 7) and paradoxically inhibit interactions known to contribute to branch formation. (*i*) Although both VCA and actin filaments are required to activate Arp2/3 complex, CA bound to high-affinity site 1 inhibits binding of Arp2/3 complex to the side of an actin filament. (*ii*) Whereas V and actin monomers contribute to branch formation, an actin monomer bound to V strongly inhibits VCA binding to free Arp2/3 complex, presumably to the high affinity. Actin bound to C may also compete with Arp2/3 complex (8). (*iii*) Although VCA contributes to nucleation by bringing a bound actin monomer to Arp2/3 complex, association of V with the barbed end of actin (6) inhibits elongation (33, 34) and VCA cross-linked to an actin monomer is a poor nucleation-promoting factor (20) (Fig. 5*C*).

Mechanism of Arp2/3 Complex Activation During Branch Formation. Our data support the idea that branch formation involves more than one interaction of VCA with Arp2/3 complex (13). We describe one possible scenario that is consistent with the available data but recognize that more information is required to verify the order of the reactions and the most populated of the many possible pathways.

VCA engages Arp2/3 complex. Cells have multiple mechanisms to cluster VCAs for parallel interactions with Arp2/3 complex: close packing of independent VCAs on cell membranes (35); tandem activity-bearing VCA motifs (12, 13); or assembly on scaffold proteins (17, 36–38) including adapters with two SH3 domains that bind proline-rich domains of two nucleation-promoting factors (NPFs) (13, 39). Activation of these crowded NPFs exposes their C-terminal VCA motifs, allowing interactions with Arp2/3 complex and actin monomers. Binding a VCA to the high-affinity site on Arp2/3 complex would favor coincident binding of a second nearby VCA to the low-affinity site.

Mother filament binding activates Arp2/3 complex. Although VCA bound to the high-affinity site inhibits binding to the side of an actin filament, VCA exchanges rapidly on and off Arp2/3 complex (Table 1), allowing Arp2/3 complex to bind a mother actin filament during intervals when VCA dissociates. Association of Arp2/3 complex with a mother filament blocks the site 1 and increases the affinity of actin-VCA for site 2 40- to 100-fold, presumably by stabilizing the active conformation found in the branch junction. Because the mother actin filaments blocks site 1, it is not occupied by VCA during subsequent steps.

Initiation of the daughter filament. Once bound to site 2 on activated Arp2/3 complex, VCA delivers the first actin subunit to the daughter filament. A second actin-VCA associated with the front side of Arp2/3 complex could deliver the second subunit of the daughter filament. We have not studied this site, but an attractive mechanism is that VCA binds with C in the barbed end groove of Arp2 (20) and with A associated with ARPC1 (39). Both of these sites are exposed when Arp2/3 complex is bound to the side of an actin filament (5).

Elongation of the daughter filament. Given the capping activity of V (33, 34) and low nucleation activity VCA cross-linked to an actin monomer (Fig. 5*C*), dissociation of VCA from the first two actin subunits will promote elongation of the daughter filament. This behavior is consistent with fluorescence recovery after photobleaching experiments, showing that rapid N-WASP exchange is critical in vivo for movements that depend on Arp2/3 complex and actin (40).

The multiple interactions in this scenario explain why dimeric GST-WASp-VCA activates Arp2/3 complex 100-fold more effectively than VCA monomers (2). Hierarchical regulation through these protein complexes and successive interactions of VCA with Arp2/3 complex are likely to contribute to the ability of cells to tune the Arp2/3 complex activity with high spatial and temporal specificity.

Our work and Padrick et al. (39) reveal that actin filament branch formation is not a simple linear pathway. Much is still to be learned about how numerous linked positive and negative interactions contribute to branch formation. Progress will require more information about CA binding sites and the massive conformational changes that bring together Arp2 and Arp3 to form the binding site for the first actin subunit in the branch.

Materials and Methods

SI Materials and Methods provides a more detailed account of our methods.

Protein Purification and Labeling. We purified Arp2/3 complex from fission yeast with modifications of a previous method (25) and measured the concentration by absorption at 290 nm ($\varepsilon = 139{,}030\ M^{-1}\ s^{-1}$). We labeled mutant Arp2/3 complex (p20 C167S p34 A317C) with *N*-(1-pyrene)iodoacetamide (p29, Invitrogen) (25). We purified bovine Arp2/3 complex from thymus (21). We expressed *S. pombe* Wsp1p-VCA (497Q–574D), *S. pombe* Wsp1-CA (542S–574D), bovine N-WASP-CA (466G–505D), and bovine N-WASP-VCA (428P–505D) as GST fusions in plasmid pGV67 in Rosetta (DE3) pLysS *Escherichia coli* cells (Novagen) and purified the proteins by ion exchange and glutathione Sepharose 4B affinity chromatography, followed by cleavage of VCA/CA from GST and Mono Q and gel filtration chromatography. We labeled a cysteine added to the N terminus of CA with Alexa-Fluor-546 C_5-maleimide (A10258, Invitrogen). The concentration of unlabeled CA was measured by absorption at 280 nm ($\varepsilon = 5{,}690\ M^{-1}\ cm^{-1}$), and the concentration of Alexa-Fluor-546-labeled CA was measured by absorption at 554 nm ($\varepsilon = 93{,}000\ M^{-1}\ cm^{-1}$). We purified actin from chicken breast muscle acetone powder by one cycle of polymerization and depolymerization followed by gel filtration on Sephacryl S-300 (41). We labeled actin Cys374 with pyrene-iodoacetamide (42) or Alexa-Fluor-488 carboxylic acid, succinimidyl ester (26). We reacted Cys-VCA with 18 mM *N*,*N*′-m-phenylenedimaleimide (PDM) in dimethylformamide for

3 h at 4 °C, removed unreacted PDM and reacted a 10-fold molar excess of PDM-VCA with Alexa-Fluor-488 actin overnight on ice. Cross-linked products were purified by gel filtration and Mono Q chromatography.

Isothermal Titration Calorimetry. We titrated 200 μL of Arp2/3 complex in the cell of a Microcal ITC 200 calorimeter (Bonsai Advanced Technologies) with 2-μL injections of 160 μM Cys-CA in 4 s each at 3-min intervals.

Crystallography. We grew small crystals of 50 μM bovine Arp2/3 complex (23) and macroseeded them into drops containing 1 μL 50 μM Arp2/3 and 1 μL well solution (100 mM Hepes 7.5, 200 mM KCl, 100 mM glycyl-glycyl-glycine and 8% PEG 8K). Crystals were soaked by adding 1 μL of 2–4 mM bovine or *S. pombe* CA to the 2 μL hanging drops for 1 h. Crystals were cryoprotected with well solution containing 25% glycerol, frozen in liquid nitrogen for storage and cryoannealed by blocking the cryostream from the sample for 3 s. X-ray diffraction data were collected at the National Synchrotron Light Source using beam line X25 equipped with an Area Detector Systems Corporation Q315 CCD detector and processed with standard methods (*SI Materials and Methods*). The coordinates of Arp2/3 complex with bound CA were submitted to the Protein Data Base, accession number 3RSE.

Viability of *S. pombe* Cells with Arp3 Mutations. We created the following substitutions in fission yeast Arp3: Arp3 P249A, P249M, P249Y, or R345A. Diploid cells with these mutations on one chromosome were sporulated on nitrogen-deficient agar plate (SPA5S) at 25 °C for 2 d. After tetrad dissection, spores grew on YE5S agar plate at 25 °C for 4 d before evaluating growth.

Spectroscopy. We used a Photon Technology International Alphascan fluorimeter to measure fluorescence intensity and fluorescence anisotropy for actin polymerization, equilibrium binding, and kinetics experiments (24).

Cross-Linking the N Terminus of VCA to Arp2. We created the following substitutions in budding yeast Arp2 and Arp3: Arp2 R198C, A207C, or D271C; Arp3 P342C or D325C. We expressed Arp2/3 complex with pairs of these substitutions in budding yeast and purified Arp2/3 complex by a method similar to that for fission yeast. Budding yeast Arp2/3 complex (2 μM) was reacted with 10 μM N-WASp-cysteine-VCA in 10 mM imidazole (pH 7.0), 50 mM KCl, 1 mM $MgCl_2$, 1 mM EGTA, 0.2 mM ATP, 0.2 mM $CaCl_2$, 50 μM $CuSO_4$ for 60 min at 4 °C. During ion exchange chromatography on Mono Q Arp2/3 complex cross-linked to VCA eluted at 40.5 mS behind free Arp2/3 complex at 31 mS.

ACKNOWLEDGMENTS. The authors thank Dorit Hanein and Rong Li for their comments on the manuscript and Shae Padrick and Michael Rosen for sharing unpublished data. We would also like to thank the staff at the Richards Center at Yale University for their software and computational support, and at the National Synchrotron Light Source for the use of beam line X25. This work was supported by National Institutes of Health Research Grants GM-026338 and GM-66311.

1. Machesky L, Insall R (1998) Scar1 and the related Wiskott–Aldrich syndrome protein, WASP, regulate the actin cytoskeleton through the Arp2/3 complex. *Curr Biol* 8:1347–1356.
2. Higgs H, Pollard T (2000) Activation by Cdc42 and PIP(2) of Wiskott–Aldrich syndrome protein (WASp) stimulates actin nucleation by Arp2/3 complex. *J Cell Biol* 150:1311–1320.
3. Kim A, Kakalis L, Abdul-Manan N, Liu G, Rosen M (2000) Autoinhibition and activation mechanisms of the Wiskott–Aldrich syndrome protein. *Nature* 404:151–158.
4. Mullins R, Heuser J, Pollard T (1998) The interaction of Arp2/3 complex with actin: Nucleation, high-affinity pointed end capping, and formation of branching networks of filaments. *Proc Natl Acad Sci USA* 95:6181–6186.
5. Rouiller I, et al. (2008) The structural basis of actin filament branching by the Arp2/3 complex. *J Cell Biol* 180:887–895.
6. Chereau D, et al. (2005) Actin-bound structures of Wiskott–Aldrich syndrome protein (WASP)-homology domain 2 and the implications for filament assembly. *Proc Natl Acad Sci USA* 102:16644–16649.
7. Panchal S, Kaiser D, Torres E, Pollard T, Rosen M (2003) A conserved amphipathic helix in WASP/Scar proteins is essential for activation of Arp2/3 complex. *Nat Struct Biol* 10:591–598.
8. Kelly A, Kranitz H, Dötsch V, Mullins R (2006) Actin binding to the central domain of WASP/Scar proteins plays a critical role in the activation of the Arp2/3 complex. *J Biol Chem* 281:10589–10597.
9. Symons M, et al. (1996) Wiskott–Aldrich syndrome protein, a novel effector for the GTPase CDC42Hs, is implicated in actin polymerization. *Cell* 84:723–734.
10. Miki H, Sasaki T, Takai Y, Takenawa T (1998) Induction of filopodium formation by a WASP-related actin-depolymerizing protein N-WASP. *Nature* 391:93–96.
11. Rohatgi R, Ho H, Kirschner M (2000) Mechanism of N-WASP activation by CDC42 and phosphatidylinositol 4, 5-bisphosphate. *J Cell Biol* 150:1299–1310.
12. Garmendia J, Carlier M, Egile C, Didry D, Frankel G (2006) Characterization of TccP-mediated N-WASP activation during enterohaemorrhagic Escherichia coli infection. *Cell Microbiol* 8:1444–1455.
13. Padrick S, et al. (2008) Hierarchical regulation of WASP/WAVE proteins. *Mol Cell* 32:426–438.
14. Castellano F, Montcourrier P, Chavrier P (2000) Membrane recruitment of Rac1 triggers phagocytosis. *J Cell Sci* 113:2955–2961.
15. Papayannopoulos V, et al. (2005) A polybasic motif allows N-WASP to act as a sensor of PIP(2) density. *Mol Cell* 17:181–191.
16. Rivera G, Briceño C, Takeshima F, Snapper S, Mayer B (2004) Inducible clustering of membrane-targeted SH3 domains of the adaptor protein Nck triggers localized actin polymerization. *Curr Biol* 14:11–22.
17. Yarar D, Waterman-Storer C, Schmid S (2007) SNX9 couples actin assembly to phosphoinositide signals and is required for membrane remodeling during endocytosis. *Dev Cell* 13:43–56.
18. Weaver A, et al. (2002) Interaction of cortactin and N-WASp with Arp2/3 complex. *Curr Biol* 12:1270–1278.
19. Pan F, Egile C, Lipkin T, Li R (2004) ARPC1/Arc40 mediates the interaction of the actin-related protein 2 and 3 complex with Wiskott–Aldrich syndrome protein family activators. *J Biol Chem* 279:54629–54636.
20. Boczkowska M, et al. (2008) X-ray scattering study of activated Arp2/3 complex with bound actin-WCA. *Structure* 16:695–704.
21. Nolen B, Littlefield R, Pollard T (2004) Crystal structures of actin-related protein 2/3 complex with bound ATP or ADP. *Proc Natl Acad Sci USA* 101:15627–15632.
22. Nolen B, Pollard T (2007) Insights into the influence of nucleotides on actin family proteins from seven structures of Arp2/3 complex. *Mol Cell* 26:449–457.
23. Robinson R, et al. (2001) Crystal structure of Arp2/3 complex. *Science* 294:1679–1684.
24. Marchand J, Kaiser D, Pollard T, Higgs H (2001) Interaction of WASP/Scar proteins with actin and vertebrate Arp2/3 complex. *Nat Cell Biol* 3:76–82.
25. Beltzner C, Pollard T (2008) Pathway of actin filament branch formation by Arp2/3 complex. *J Biol Chem* 283:7135–7144.
26. Mahaffy R, Pollard T (2006) Kinetics of the formation and dissociation of actin filament branches mediated by Arp2/3 complex. *Biophys J* 91:3519–3528.
27. Zalevsky J, Grigorova I, Mullins R (2001) Activation of the Arp2/3 complex by the Listeria acta protein. Acta binds two actin monomers and three subunits of the Arp2/3 complex. *J Biol Chem* 276:3468–3475.
28. Zalevsky J, Lempert L, Kranitz H, Mullins R (2001) Different WASP family proteins stimulate different Arp2/3 complex-dependent actin-nucleating activities. *Curr Biol* 11:1903–1913.
29. Zencheck W, et al. (2009) Nucleotide- and activator-dependent structural and dynamic changes of arp2/3 complex monitored by hydrogen/deuterium exchange and mass spectrometry. *J Mol Biol* 390:414–427.
30. Nolen B, Pollard T (2008) Structure and biochemical properties of fission yeast Arp2/3 complex lacking the Arp2 subunit. *J Biol Chem* 283:26490–26498.
31. Volkmann N, et al. (2001) Structure of Arp2/3 complex in its activated state and in actin filament branch junctions. *Science* 293:2456–2459.
32. Egile C, et al. (2005) Mechanism of filament nucleation and branch stability revealed by the structure of the Arp2/3 complex at actin branch junctions. *PLoS Biol* 3:e383.
33. Egile C, et al. (1999) Activation of the CDC42 effector N-WASP by the Shigella flexneri IcsA protein promotes actin nucleation by Arp2/3 complex and bacterial actin-based motility. *J Cell Biol* 146:1319–1332.
34. Higgs H, Blanchoin L, Pollard T (1999) Influence of the C terminus of Wiskott–Aldrich syndrome protein (WASp) and the Arp2/3 complex on actin polymerization. *Biochemistry* 38:15212–15222.
35. Footer M, Lyo J, Theriot J (2008) Close packing of Listeria monocytogenes ActA, a natively unfolded protein, enhances F-actin assembly without dimerization. *J Biol Chem* 283:23852–23862.
36. Coppolino M, et al. (2001) Evidence for a molecular complex consisting of Fyb/SLAP, SLP-76, Nck, VASP and WASP that links the actin cytoskeleton to Fcgamma receptor signalling during phagocytosis. *J Cell Sci* 114:4307–4318.
37. Ho H, et al. (2004) Toca-1 mediates Cdc42-dependent actin nucleation by activating the N-WASP-WIP complex. *Cell* 118:203–216.
38. Tehrani S, Tomasevic N, Weed S, Sakowicz R, Cooper J (2007) Src phosphorylation of cortactin enhances actin assembly. *Proc Natl Acad Sci USA* 104:11933–11938.
39. Padrick SB, Doolittle LK, Brautigam CA, King DS, Rosen MK (2011) Arp2/3 complex is bound and activated by two WASP proteins. *Proc Natl Acad Sci USA*, 10.1073/pnas.1100236108.
40. Weisswange I, Newsome T, Schleich S, Way M (2009) The rate of N-WASP exchange limits the extent of ARP2/3-complex-dependent actin-based motility. *Nature* 458:87–91.
41. MacLean-Fletcher S, Pollard T (1980) Identification of a factor in conventional muscle actin preparations which inhibits actin filament self-association. *Biochem Biophys Res Commun* 96:18–27.
42. Pollard T (1984) Polymerization of ADP-actin. *J Cell Biol* 99:769–777.